PHYSICAL REVIEW A **84**, 041803(R) (2011)

Light emission of a scarlike mode with assistance of quasiperiodicity

Chang-Hwan Yi,[1] Sang Hun Lee,[2] Myung-Woon Kim,[1] Jinhang Cho,[1] Jinhyung Lee,[1] Soo-Young Lee,[3] Jan Wiersig,[4] and Chil-Min Kim[1,*]

[1]*Department of Physics, Sogang University, Seoul 121-742, Korea*
[2]*Department of Physics, Seonam University, Namwon, Jeonbuk 590-711, Korea*
[3]*Department of Physics, Pusan National University, Dongrae-Gu, Busan 609-735, Korea*
[4]*Institut für Theoretische Physik, Otto-von-Guericke-Universität Magdeburg, D-39016 Magdeburg, Germany*

(Received 7 June 2011; published 10 October 2011)

In an elliptic $In_xGa_{1-x}AsP$ microcavity laser, various scarlike modes are experimentally observed. Below the lasing threshold, a bouncing-ball, a triangle, a double, and a triple bow-tie mode spontaneously emit. Above the threshold, a bow-tie scarlike mode lases alone. Our numerical analysis reveals that the bow-tie scarlike mode is not caused by regular islands in phase space due to the Goos-Hänchen shift, but by unstable periodic orbits and that the light emission is assisted by a quasiperiodic orbit.

DOI: 10.1103/PhysRevA.84.041803 PACS number(s): 42.55.Sa, 42.55.Px, 05.45.Mt

In a closed chaotic system, some quantum energy eigenfunctions are localized on unstable periodic orbits of the underlying classical system [1]. These eigenfunctions, named scars, are widely observed in various systems such as quantum dots, hydrogen atoms, microwave, and optical microcavities [2,3]. The latter kind of systems is of particular interest, as these systems are open due to the emission of light. The quasibound states (modes, resonances) in chaotic dielectric microcavities have been analyzed based on the scar theory and resonances localized along periodic orbits (ray trajectories) have been found [4,5]. In nonchaotic systems like circular, elliptic, and rectangular dielectric microcavities, it has been considered that there is no scarred resonance.

Recently, two kinds of abnormal scarred resonances were found in dielectric microcavities: a quasiscarred resonance (QSR) [6,7] and a scarlike resonance (SLR) [8]. In a spiral-shaped dielectric cavity, the mode pattern often shows a simple geometrical structure of a triangle and a star shape depending on the refractive index. Because such a state cannot be found in the corresponding closed cavity (so-called billiard), the QSR is the resonance appearing in an open system. The QSR was also experimentally observed [9]. In the case of the SLR, although a rectangular and an elliptic cavity are not chaotic, the resonances are localized along a periodic orbit due to avoided resonance crossings appearing in open systems. The SLR is analyzed by using the Goos-Hänchen shift [10], which perturbs the integrable system to create chaotic regions and islands in the reduced phase space (S, $\sin\chi$), that is the Poincaré surface of section, where S is the arc length and χ is the angle of incidence. The SLRs were explained by localization of modes on the islands and on unstable periodic orbits. Yet the SLR is not observed in an experiment.

In this Rapid Communication, we report an experimental observation of various SLRs in an elliptic $In_xGa_{1-x}AsP$ microcavity laser. Below the lasing threshold, spontaneous emission from SLRs of a bouncing ball, a triangle, a double bow tie, and a triple bow tie are observed. Above the threshold, a bow-tie SLR is the lasing mode. In a numerical analysis, we reveal that the bow-tie SLR is not caused by islands due to Goos-Hänchen shift but due to an unstable periodic orbit and that the laser emission of the bow-tie SLR is assisted by quasiperiodicity.

The elliptic microcavity laser is fabricated with $In_xGa_{1-x}AsP$, whose effective refractive index is $n_e = 3.3$. The radius of the major and the minor axis is $a = 95\ \mu$m and $b = 30\ \mu$m, respectively, with the aspect ratio $b/a = 0.317$. The size of the cavity is about $n_e kL/2\pi \sim 873$ for the wavelength of $\lambda = 1575$ nm, where k is the wave number and L is the boundary length. The fabrication process and parameters are the same as in Ref. [11]. The light emission is launched into a fiber, whose facet is spherical, and the emission intensity is measured with a power detector (Newport 818-IR) connected to a multifunction optical meter (Newport 1835C) and the spectrum with an optical spectrum analyzer (Agilent 86142B).

Figure 1 shows the emission intensity depending on the injection current. In the measurement, the fiber, which is 50 μm apart from the boundary, is faced to the major axis. In the figure, the emission intensity increases slowly below 60 mA and it grows up rapidly above 60 mA. Hence the lasing threshold is around 60 mA.

For the two cases of the injection current, below and above the threshold, the emission spectra are obtained around the boundary. In the measurement, the fiber facet is 30 μm apart from the boundary. At 55 mA, we obtain spontaneously emitting four mode groups according to the measurement angle. At the minor axis, an equidistantly spaced mode group emits with mode spacing of about 5.37 nm; see Fig. 2(a). At 60° from the major axis, a different mode group emits as shown in Fig. 2(b), whose mode spacing is about 1.33 nm. At 30°, the mode spacing is 1.56 nm; see Fig. 2(c). Around the major axis, the mode spacing is about 1.73 nm as shown in Fig. 2(d). When the injection current increases up to 59.2 mA, another mode group begins to emit around the major axis. Figure 2(e) displays the lasing mode group at 62 mA. From the five peaks in the range from 1570 to 1580 nm, the average mode spacing of about 1.695 nm is obtained. The peaks are narrow enough as the evidence of lasing. On a further increase of the current, the intensity of the mode group in Fig. 2(e) increases alone.

*chmkim@sogang.ac.kr

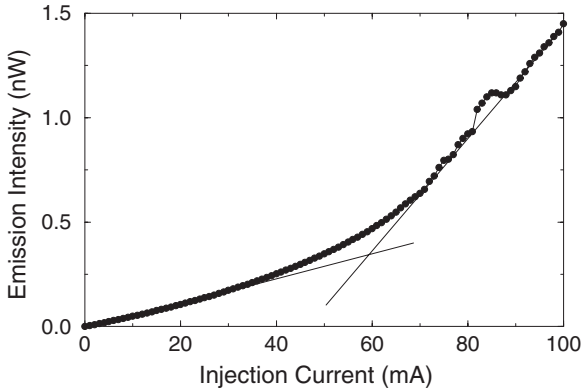

FIG. 1. Total emission intensity around the major axis depending on the injection current.

From the equation $l = \lambda^2/\Delta\lambda n_g$, the path length l can be obtained, where λ is the average wavelength of the two neighboring modes, $\Delta\lambda$ is the mode spacing of two neighboring modes, and n_g is the group refractive index. Also, when the path length is known, n_g can be determined. The mode spacing of 5.37 nm in Fig. 2(a) is the bouncing-ball-type mode traveling along the minor axis because there is no such large mode spacing except the bouncing ball. Although the mode is not lasing, $n_g = 3.68$ is obtained from 17 peaks. This value of n_g is confirmed in another elliptic cavity, whose minor axis radius is 50 μm. The obtained n_g is also similar to what was observed elsewhere in $In_xGa_{1-x}AsP$ semiconductor lasers [12].

When we apply $n_g = 3.68$, the path length of the mode group in Figs. 2(b), 2(c), and 2(d) is about 498, 433, and 389 μm. The lengths correspond to the path lengths of the

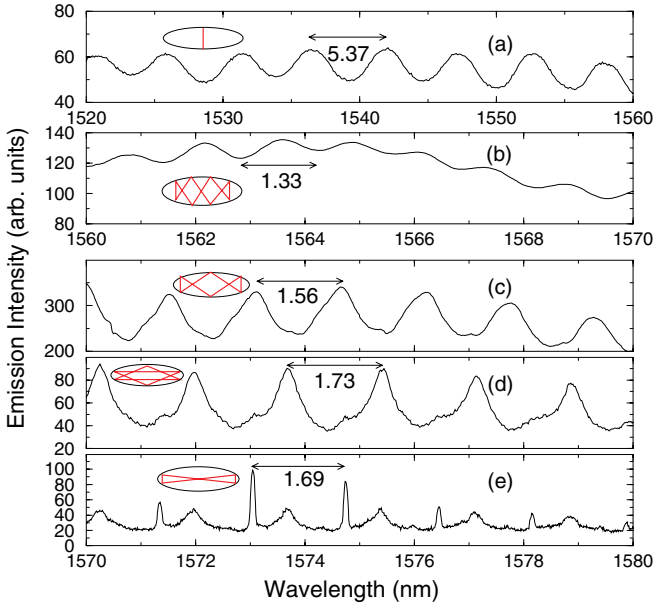

FIG. 2. (Color online) Optical spectra; (a) is the emission spectrum at minor axis (bouncing ball), (b) is at 60° from the major axis (triple bow tie), (c) is at 30° (double bow tie), and (d) is around the major axis (triangle) at 55 mA injection current. (e) The laser emission around the major axis (bow tie) at 62 mA. The insets are the diagrams of the relevant trajectories.

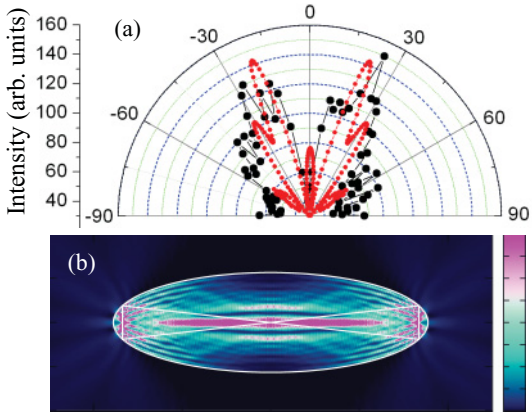

FIG. 3. (Color online) Far field pattern and measured angle; (a) the black line is the experimental result at 62 mA and the red line is the numerical result of the bow-tie SLR shown in (b). (b) The resonance of the bow-tie SLR for $nkL/2\pi \approx 163$. The resonance point is $\mathrm{Re}(kL/2\pi) = 49.40$ and $\mathrm{Im}(kL/2\pi) = -0.02$.

triple bow-tie (497.2 μm), the double bow-tie (434.2 μm), and the triangle SLR (387.3 μm) as shown by the insets in Fig. 2. The path length of the lasing mode group shown in Fig. 2(e) is about 398 μm within 0.1% accuracy, which nicely corresponds to the path length of the bow-tie SLR of 398.1 μm. We focus our attention on the emission of the bow-tie SLR. At 62 mA injection current, the angular dependence of the far-field pattern is measured as shown by the black line in Fig. 3(a). The fiber facet is 50 μm apart from the boundary, which is about half of the major axis radius, that is $a/2$. The figure shows two strong emission directions around $\pm 25°$. To confirm the emission direction, we obtain the bow-tie SLR by the boundary element method [13] for $nkL/2\pi \sim 163$ as shown in Fig. 3(b), whose real and imaginary normalized frequencies are $\mathrm{Re}(kL/2\pi) \sim 49.40$ and $\mathrm{Im}(kL/2\pi) \sim -0.002$. Although the size is 5.3 times smaller than the experimental one, we can qualitatively confirm the emission direction. The obtained resonance is well fitted to the bow-tie ray trajectory. From the bow-tie SLR, we extract the emission direction by taking the emission intensity along the boundary apart from a half of the major axis radius ($a/2$) according to the experimental measurement. The emission direction of the red line shown in Fig. 3(a) well coincides with the experimental result. Hence, from the emission direction and the mode spacing, we can confirm the lasing of the bow-tie SLR in a highly deformed elliptic microcavity laser.

In the analysis of ray dynamics including the Goos-Hänchen shift, we cannot find any regular islands in phase space related to the bow-tie trajectory but, instead, we find unstable periodic orbits. This seems to be in contradiction to the numerically computed mode pattern shown in Fig. 4(d). To resolve this apparent contradiction, we compute a survival probability distribution (SPD) [6] for $n_e = 3.3$, neglecting the small Goos-Hänchen shift. Since our laser generates transverse electric (TE) polarized modes, the SPD is obtained by using 10^8 initial rays and TE polarization for the reflection coefficients. The phase space $(S/S_{\max}, P = \sin\chi)$ is divided into 1000×1000 cells and the survived intensity of the rays from 200 to 300 time steps is accumulated, where one time

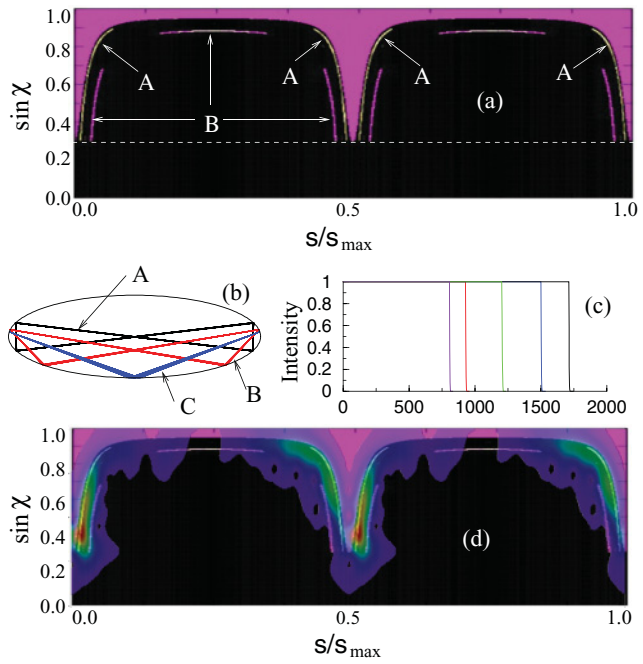

FIG. 4. (Color online) (a) SPD, where A and B denote the faint lines of a bow-tie and a double bow-tie resonance mode, respectively. S is the arc length from right major axis and χ is the incident angle. (b) The transition from the bow-tie trajectory to a V type in an elliptical cavity, where black is in between 0 and 100 time steps, red is in between 1600 and 1700 time steps, and blue is in between 2900 and 3000 time steps. (c) The decay time of the rays for five different initial values near the bow-tie trajectory. (d) The emerging Husimi function on the SPD.

step is the normalized time to pass the ray on the major axis. Figure 4(a) shows the SPD, where 10 faint lines exist. Since the ellipse is an integrable system, there is no chaotic sea but instead only quasiperiodic orbits. The faint lines originated from these quasiperiodic orbits. The lines labeled by A and B correspond to the bow-tie and the double bow-tie SLR, respectively. The other lines, which correspond to the experimentally observed SLRs, cannot be found in the SPD because they escapes from the cavity rapidly due to the small value of the incident angle.

To show that the faint lines are related to the SLRs, the trajectory variation and decay times of rays are determined. Figure 4(b) shows the trajectory variation from a bow-tie to a V type when the deviation of the initial values from the unstable periodic orbits of the bow-tie trajectory is about $\Delta S = 5.53 \times 10^{-5}$ and $\Delta P = 2.36 \times 10^{-4}$. 1700 time steps later, the bow-tie trajectory shown by the black line transits to the red trajectory. 2900 time steps later, the red trajectory transits to the V type trajectory as shown by the blue trajectory. We note here that the V type trajectory transits to the Λ type through the bow-tie trajectory. The variation of the trajectory is caused by the quasiperiodic orbits in the elliptic cavity. In our case, since the smallest incident angle of the bow-tie trajectory is larger than the critical angle for total internal reflection, the rays cannot escape from the cavity. During the variation, when the incident angle becomes the critical angle, that is, the trajectory touches the critical line in phase space, the rays escape from the cavity. This is the emission of the bow-tie SLR. Because it takes a long time for the incident angle of the bow-tie trajectory to come close to the critical angle, the faint lines exists in phase space.

Figure 4(c) shows the decay times of rays for five different initial values around the bow-tie trajectory. The decay time reaches to 1700 time steps for the initial value of Fig. 4(b). The decay time is taken for the trajectory to transit from the black to the red trajectory. The closer the initial point to the unstable periodic orbit of the bow-tie trajectory is, the longer the decay time is. Because the smallest incident angle of the bow tie and double bow tie of 41.77° and 31.46° is larger than the critical angle of 17.64°, the ray cannot escape from the cavity until the incident angle is less than the critical angle leading to the faint lines in the SPD. However, because the incident angle of the triple bow-tie and the triangle SLR of 17.54° and 9.26° is less than the critical angle, the faint lines for them do not exist.

Figure 4(d) is the emerging Husimi function (the projection of a mode onto the Poincaré surface of section [14]) of the bow-tie SLR superimposed onto the SPD. The function is well matched to the faint lines of the bow-tie trajectory. The high intensity region is overlapped with the faint lines and the function touches the critical line. This is another evidence of the lasing of the bow-tie SLR with the assistance of the quasiperiodicity.

The faint lines are the route for the bow-tie SLR to emit light. This phenomenon is similar to that of lasing emission due to chaos-assisted tunneling in chaotic cavities [15–18], where light tunnels from a regular island around a stable periodic orbit to the neighboring chaotic sea and escapes from the cavity by following the unstable manifolds. In our case, the elliptic cavity is an integrable system having only quasiperiodic orbits. When a light beam has a Gaussian profile, the light around the unstable periodic orbit of the bow tie follows the nearby quasiperiodic orbits. Hence the bow-tie SLR should emit when the trajectory becomes the red one in Fig. 4(b). Similar behavior was observed in a hexagonal cavity [19].

The experimentally obtained modes are the very SLRs because an elliptic billiard cavity does not exhibit scarred modes. In previous experimental studies of an elliptic cavity, not these modes but whispering gallery modes were found when the aspect ratio is larger, that is, the cavity is not much deformed [20–22]. The difference between our results and the others relies on the aspect ratio and the refractive index. The modes in an elliptic billiard can be classified into two types: bouncing ball and whispering gallery. The two types are distinguished by the foci of the ellipse, whether a trajectory goes between the two foci or not [23]. The bow-tie SLR belongs to the bouncing-ball type. When the aspect ratio is large enough for the incident angle to be less than the critical angle, the bow-tie SLR cannot be a lasing mode in a dielectric microcavity because the losses are too high. Then a whispering gallery mode emits. When the aspect ratio is small, that is, the incident angle of a bow-tie SLR is larger than the critical angle, the bow-tie SLR can emit. According to our further numerical studies, as the aspect ratio increases, the faint lines for the double bow tie disappear first. For example, when the aspect ratio is 0.5, we can find the faint lines of the bow tie only, but

not those of the double bow tie. On a further increase of the aspect ratio, the faint lines of the bow tie disappear as well. We confirm the disappearance when the aspect ratio is 0.7. Thus we can speculate that the lasing of the bow-tie SLR in elliptic cavities is caused by the small aspect ratio, by which the faint lines exist to assist the lasing through the quasiperiodic orbit.

In the analysis, by using the Poincaré surface of section including Goos-Hänchen shift, we find many small islands corresponding to the diamond, the rectangular SLR, etc. However, to emphasize, the islands corresponding to the bouncing-ball-type SLRs like the bow tie, double bow ties, etc. cannot be found. Hence we can say that the islands supporting bouncing-ball-type SLRs do not exist in an elliptic cavity, but the SLRs are caused by the unstable periodic orbits.

In conclusion, various SLRs are experimentally observed in an elliptic-shaped $In_xGa_{1-x}AsP$ semiconductor microcavity laser, whose aspect ratio is 0.317. As the evidence, the accurate path length is obtained from the mode spacing by considering the group refractive index. Especially, in the case of a bow-tie SLR, the resonance is computed by the boundary element method and the experimentally obtained emission direction well coincides with that of the resonance. We also show that the bow-tie SLR is not supported by islands, but by unstable periodic orbits. The emission is assisted by the quasiperiodic orbit of the bow tie, although the mode is confined in the cavity by total internal reflection.

This work is supported by Acceleration Research (Center for Quantum Chaos Application) of MEST/NRF. J.W. also acknowledges financial support from the DFG research group 760. We also thank Dr. K. R. Oh and J. H. Kim, for the fabrication of the laser and valuable discussions.

[1] E. J. Heller, Phys. Rev. Lett. **53**, 1515 (1984).
[2] *Optical Microcavities*, edited by K. Vahala (World Scientific, Singapore, 2004).
[3] H. J. Stöckmann, *Quantum Chaos: An Introduction* (Cambridge University Press, London, 2000).
[4] J. U. Nöckel and A. D. Stone, Nature (London) **385**, 45 (1997).
[5] C. Gmachl *et al*., Science **280**, 1556 (1998).
[6] S. Y. Lee *et al*., Phys. Rev. Lett. **93**, 164102 (2004).
[7] J. Lee, S. Rim, J. Cho, and C. M. Kim, Phys. Rev. Lett. **101**, 064101 (2008).
[8] J. Wiersig, Phys. Rev. Lett. **97**, 253901 (2006).
[9] C. M. Kim, S. H. Lee, K. R. Oh, and J. H. Kim, Appl. Phys. Lett. **94**, 231120 (2009).
[10] J. Unterhinninghofen, J. Wiersig, and M. Hentschel, Phys. Rev. E **78**, 016201 (2008).
[11] C. M. Kim, J. Cho, J. Lee, S. Rim, S. H. Lee, K. R. Oh, and J. H. Kim, Appl. Phys. Lett. **92**, 131110 (2008).
[12] G. Belenky *et al*., IEEE Photon. Tech. **12**, 969 (2000).
[13] J. Wiersig, J. Opt. A: Pure Appl. Opt. **5**, 53 (2003).
[14] M. Hentschel, H. Schomerus, and R. Schubert, Europhys. Lett. **62**, 636 (2003).
[15] M. J. Davis and E. J. Heller, J. Chem. Phys. **75**, 246 (1981).
[16] G. Hackenbroich and J. U. Nöckel, Europhys. Lett. **39**, 371 (1997).
[17] V. A. Podolsky and E. E. Narimanov, Opt. Lett. **30**, 474 (2005).
[18] S. Shinohara *et al*., Phys. Rev. Lett. **104**, 163902 (2010).
[19] J. Wiersig, Phys. Rev. A **67**, 023807 (2003).
[20] J. Manning, R. Olshansky, and C. B. Su, IEEE J. Quantum Electron. **QE-19**, 1525 (1983).
[21] S. K. Kim, S. H. Kim, G. H. Kim, H. G. Park, D. J. Shin, and Y. H. Lee, Appl. Phys. Lett. **84**, 861 (2004).
[22] S. Sunada, T. Harayama, and K. S. Ikeda, Opt. Lett. **29**, 718 (2004).
[23] H. Waalkens, J. Wiersig, and H. R. Dullin, Ann. Phys. (NY) **260**, 50 (1997).